Transport Characteristics of Suspensions: Part IX.

Representation of Periodic Phenomena on a Flow Regime Diagram for Dilute Suspension Transport

DAVID G. THOMAS

Oak Ridge National Laboratory, Oak Ridge, Tennessee

Four different flow regimes may be identified during transport of dilute suspensions of solid particles through horizontal pipes by liquids in turbulent flow as the velocity is varied. The regimes may be characterized by the distribution of solids in the channel. In two of the regimes the bulk of the material is immediately adjacent to the bottom of the channel and is clumped up either into transverse waves (dunes or islands) with a reproducible periodicity or into longitudinal waves (long stria). The definition of the other two regimes is somewhat more arbitrary but may qualitatively be described as heterogeneous or homogeneous flow. Extensive studies of the conditions under which transverse and longitudinal waves occurred, when combined with results of previous studies, showed that all four of these flow regimes may be conveniently represented on a single diagram in which the terminal-settling velocity divided by the friction velocity and the Reynolds number on particle diameter and friction velocity are the coordinates. Because the particle Reynolds number based on the terminal-settling velocity can be uniquely defined as an additional parameter on such a diagram the particular flow behavior for any given combination of system and particle characteristics can be readily determined.

When solids with a density greater than water are transported through a horizontal conduit, the distribution of particles in a vertical cross section is determined by complex interactions between the turbulent fluid and the particles. Rigorous solutions to many particle distribution problems of interest are unavailable at the present time despite numerous theoretical studies (*1* to *7*, *36*, *37*), extensive experimental work in connection with pneumatic and hydraulic transport in pipes (*8*, *34*, *35*), and studies of sediment transport in alluvial channels (*9*). One important problem is the prediction of the flow regime to be expected for a particular combination of particle characteristics, system geometry, and flow conditions.

During extensive studies of flow phenomena in suspension transport transverse sediment wave formation with a definite and reproducible periodicity was observed on the bottom of horizontal pipes. Although the sediment waves have rarely been reported in round pipes running full of liquid, they are clearly related to dune and ripple formation in alluvial channels(*10*). However little information is available on either the flow conditions required to cause particles of a given size and density to clump together into transverse waves or on the range of conditions for which these waves exist (*10*). The present studies also showed that longitudinal waves (which were observed on long irregular stria on the bottom of the pipe moving in the direction of flow) occurred after the breakup of the transverse waves and before the onset of the minimum transport condition.

The object of this paper is to develop a flow regime diagram for particle transport by combining the results from minimum transport correlation given previously (*11*) with the new data on sediment wave formation obtained at flow velocities less than the minimum transport condition and with data from prior studies on sediment and particle transport. The resultant flow regime diagram will provide a means for describing the distribution of particles in a vertical cross section of a horizontal pipe for any given combination of particles and system characteristics. The flow regime diagram will serve the additional purpose of supplying a framework in which the various flow phenomena defined by previous authors can be compared in order to arrive at a consistent set of primary definitions.

BASIC CONCEPTS

The two extremes of particle distribution are flow of the fluid over a stationary bed of particles and flow with the particles uniformly distributed over a vertical cross section of the conduit. The first case can be achieved by reducing the fluid velocity to an arbitrarily low value, but there is some doubt (*12*) that the latter case can be achieved under any except special circumstances (*10*). This paper is concerned with flow regimes between these two extremes. Starting with the lowest fluid velocity and a stationary bed of particles the following distributions of particles may be identified as the velocity is increased.

1. Periodic disposition of material on the bottom of the pipe. These transverse waves or dunes have the appearance of discrete clumps or islands of sediment particles when they are observed in round pipes. The waves creep along the bottom of the pipe in the direction of flow and have a reproducible wave length, height, and velocity.
2. Longitudinal waves (ribbons or stria of sediment

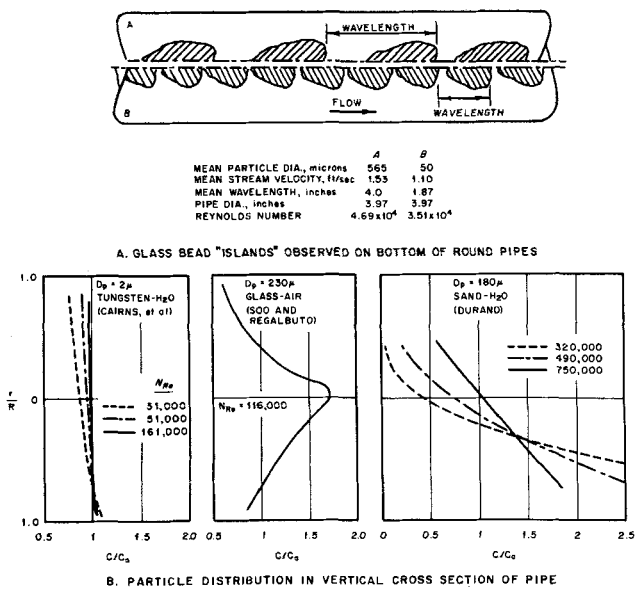

Fig. 1. Particle distribution observed in suspension transport.

particles) which, although somewhat unstable, characteristically have dimensions approximately 0.1-pipe diameters wide and 1 to 3 pipe diameters long as they are transported in the direction of flow.

3. Heterogeneous flow whose lower limit is given by the minimum transport condition (defined as the mean-stream velocity required to prevent the accumulation of a layer of stationary or sliding particles on the bottom of a round horizontal conduit). The minimum transport velocity is always sufficient to prevent longitudinal concentration gradients but, depending on particle size, may not be sufficiently large to prevent vertical concentration gradients due to the action of gravity on the particulate matter (*11*). The minimum transport velocity V_m is commonly identified with the minimum in the $(\Delta h/L)$ vs. velocity curves (*11*, *13* to *15*), while the velocity at which the suspension head loss curve joins the line for the pure suspending medium is often termed the standard velocity V_s.

4. Fully suspended flow in which the particulate matter is uniformly and homogeneously distributed throughout the cross section of a horizontal pipe. [In all probability this regime cannot be realized in practice since it is approached exponentially (*10*)].

An appreciation for these different distributions can be obtained from the data shown in Figure 1. The upper portion of the figure illustrates island formation at velocities below V_m for two particle sizes. The curves in the lower portion (B) of the figure show the effect of particle size and fluid medium on particle distribution at velocities greater than V_m. For the 2-μ particles in water (*17*), the minimum transport velocity is calculated to correspond to a Reynolds number of 28,000; at a Reynolds number of 31,000 (only 10% greater than this value) Figure 1B shows that the small particle size suspension is relatively uniformly distributed throughout the pipe. On the other hand the minimum transport velocity for the 180-μ particles (*14*) corresponds to a Reynolds number of 2.8×10^5, and at a 10% higher Reynolds number (320,000) Figure 1B shows that there is a marked concentration gradient. The standard velocity for the 180-μ particles, estimated from Gibert's data (*18*), corresponds to a Reynolds number of 6.4×10^5; Figure 1B shows that even under these conditions the distribution of particles is far from uniform. Finally the differences between concentration distributions obtained with air and water as the fluid can be seen by comparing Durand's data (*14*) with those of Soo and Regalbuto (*12*). The differences in behavior are probably due to the large differences in particle-fluid density ratio (*16*); as a result particles can bounce several orders of magnitude higher in a gas-solid system than in a liquid-solid system, thus spending more time in the high velocity central core region of the pipe.

Previous papers in this series (*11*) have dealt with the minimum velocity for transport of solids in round horizontal pipes. In these papers the minimum transport correlation was arrived at empirically by extrapolating to zero concentration with the concentration dependence accounted for by separate expressions. The results of these studies showed that the minimum transport condition at infinite dilution was described by two different relations, depending on whether the particles were smaller or greater than the thickness of von Karman's postulated laminar sublayer:

$$\delta = 5\,\nu/u^* \tag{1}$$

Thus for $D_p/\delta < 1$

$$\frac{U_t}{u^*_{om}} = 0.010 \left(\frac{D_p\, u^*_{om}}{\nu} \right)^{2.71} \tag{2}$$

while for $D_p/\delta > 1$

$$\frac{U_t}{u^*_{om}} = 4.90 \left(\frac{D_p\, u^*_{om}}{\nu} \right) \left(\frac{\nu}{D\, u^*_{om}} \right)^{0.60} \left(\frac{\rho_p - \rho}{\rho} \right)^{0.23} \tag{3}$$

This mean deviation of the data from these equations was less than 25% over a wide range of experimental conditions. The form of Equations (2) and (3) suggested that a convenient form for presenting suspension transport data would be as a log-log plot of (U_t/u^*_o) vs. $D_p\, u^*_o/\nu$. These coordinates were also used in correlating data for the beginning of bed load movement in alluvial channels (*9*). The principle advantage of this form of flow regime diagram is the information it offers about the flow patterns experienced by the individual particles. For instance for $(D_p\, u_o^*/\nu) < 5$ a particle in contact with the channel wall would be immersed in an essentially laminar sublayer with the minimum transport velocity being given by Equation (2). For $(D_p\, u_o^*/\nu) > 5$ a particle resting on the channel wall would extend into a region where appreciable fluctuating radial components of velocity occur. In this case the minimum transport velocity is given by Equation (3). In addition the diagonal lines for constant values of the product $(D_p\, u_o^*/\nu)\ (U_t/u_o^*) = D_p\, U_t/\nu$ give the Reynolds number (and hence the drag coefficient) for particles settling in a quiescent fluid.

EXPERIMENTAL EQUIPMENT AND PROCEDURE

The segregation of spherical particles into transverse and longitudinal moving deposits was studied in the 1- and 4-in. diameter glass pipe loops previously described (*11*). The fluid flow rate was adjusted with either a variable speed drive on the pump or with a bypass line. That the formation of waves was unaffected by vibrations from the pump was shown by the fact that the wave length of the islands of particles at any given velocity was independent of the combination of pump speed or bypass line setting used to achieve this velocity. Wave formation was also studied in a horizontal glass loop of ¼-in. I.D. in which the liquid was fed from a constant head tank completely isolated from the pump, thus eliminating any effect of pump vibrations on wave formation.

Before a test was begun, solids were distributed uniformly along the bottom of the pipe by operating at greater than the minimum transport velocity; the flow rate was then reduced to permit deposition of all particles. With a layer of immobile particles from 1/16- to 1/8-pipe diameters deep on the bottom of the pipe and with a very low flow rate the fluid velocity was increased to the desired value, and within seconds the particles began to segregate into transverse waves (dunes or islands as shown in the upper portion of Figure 1) or into longitudinal

TABLE 1. PROPERTIES OF PARTICLES USED IN STUDY OF WAVE FORMATION

Material	Nominal size range in terms of U.S. std. mesh size	Mean diameter, μ	Terminal-settling velocity at 70°F., ft./sec.
Glass	−16 + 25	950	0.46
Glass	−25 + 40	565	0.27
Glass	−40 + 60	335	0.16
Glass	−60 + 100	200	0.074
Glass	−100 + 230	105	0.025
Glass	−150 + 270	78	0.016
Glass	−140	50	0.0065
Ion exchange	−10 + 30	507	0.029
Ion exchange	−70 + 100	180	0.0052

waves or stria. Flow rates were meaured with a weigh tank; in all cases the suspensions were sufficiently dilute that measurements of the head loss were the same as those for smooth pipes within the precision of the water manometers. Sufficient tests were run with each size of particle to delineate the range of velocities in which the different types of wave formation existed.

Particles of two different densities were used in these studies, glass beads and ion exchange resins with densities of 2.65 and 1.09 g./cc., respectively (Table 1). Care must be used in determining the characteristics of the ion exchange materials since they may swell appreciably (*19*). In the present study the resin was treated with 0.1-N sodium chloride solution and washed with water before the tests. The particle size and settling rates of these materials were then used to calculate the density given in Table 1.

EXPERIMENTAL RESULTS

Data for the range of conditions in which longitudinal and transverse waves may exist in round horizontal pipes are shown in Figure 2. The open points, which define the lower limit of velocity for the formation of transverse waves, were obtained by linear extrapolation on a plot of island or wave velocity vs. friction velocity, u_o^*. This lower limit proved to be independent of pipe diameter, and the particle density was satisfactorily accounted for by the use of the terminal-settling velocity in the ordinate of Figure 2. Details of the relation between island velocity, wave length and height, and the mean stream velocity are described elsewhere (*33*).

The upper limit on velocity for transverse wave formation was determined by visual observation and was also found to be independent of pipe diameter. However the data on ion exchange resins indicated that the effect of particle density was no longer accounted for by the terminal-settling velocity term in the region $D_p u_o^*/\nu > 5$ but that a small additional correction for density was required. The limited data indicate that the correction is given by

$$U_t/u_o^* = \left(\frac{\rho}{\rho_p - \rho}\right)^{0.33} \psi\,(D_p u_o^*/\nu) \qquad (4)$$

Figure 2 also contains the curve given by Shields (*20*) for the beginning of bed load movement in alluvial channels and the curve proposed by Liu (*21*) for the beginning of ripple formation in alluvial channels. The data given by Zenz (*22*) for the minimum velocity for transport of a single particle in a liquid medium without saltation and without obviously rolling or bouncing are shown in Figure 2 as solid black circles. The present data on beginning of transverse wave formation in round pipes are in remarkably good agreement with the data of Shields for beginning of bed load movement in alluvial channels

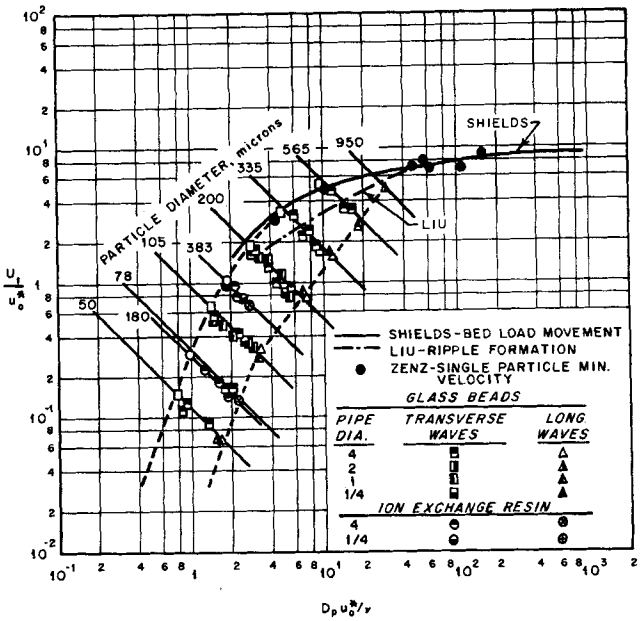

Fig. 2. Experimental determination of flow regimes for longitudinal and transverse waves.

and with the data of Zenz for single particle minimum transport velocity in round horizontal pipes. The curve presented by Liu would be in excellent agreement with the data cited above if it were drawn as an envelope dividing the regime for no ripple observation from the regime where ripples were observed rather than through the mean of the data as was actually done. Thus all these data appear to specify the same unique curve whose location defines flow phenomena observed under a wide variety of conditions, and the different names used in different studies all refer to a common condition.

GENERALIZED FLOW REGIME DIAGRAM

A generalized flow regime diagram for suspension transport may be prepared by combining the results of Figure 2 and Equations (2) and (3). A typical example is shown in Figure 3 for a system having a density ratio $(\rho_p - \rho)/$

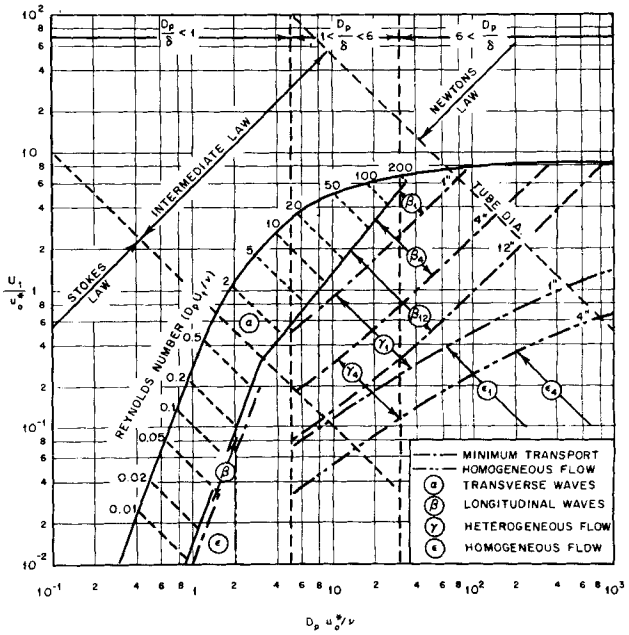

Fig. 3. Generalized phase diagram for suspension transport. [Range of β, γ, and ϵ phases apply to density ratio $(\rho_p - \rho)/\rho = 1.65$.]

$\rho = 1.65$. In the upper portion of the figure the limits for the size of particle relative to the thickness of the laminar sublayer [Equation (1)] and the buffer layer as defined by von Karman (23) are shown by the lines $D_p/\delta < 1$ and $1 < D_p/\delta < 6$, respectively. The two diagonal dotted lines separate the regions where particles settle in a quiescent fluid in accordance with Stokes' law ($D_p U_t/\nu < 1$)

$$U_t = \frac{g_L (\rho_p - \rho) D_p^2}{18 \mu} \tag{5}$$

the intermediate law [$1 < (D_p U_t/\nu) < 500$]

$$U_t = \frac{0.153 g_L^{0.71} D_p^{1.14} (\rho_p - \rho)^{0.71}}{\rho^{0.29} \mu^{0.43}} \tag{6}$$

and Newton's law ($500 < D_p U_t/\nu$)

$$U_t = 1.74 \sqrt{\frac{g_L D_p (\rho_p - \rho)}{\rho}} \tag{7}$$

For a given system these 45-deg. lines represent constant particle size; consequently as the fluid velocity is increased, the data fall along these lines from the upper left to the lower right. For convenience the values of the Reynolds number ($D_p U_t/\nu$) are given from 0.01 to 200.

The four different regimes of dilute suspension transport will be identified as: α = transverse waves, β = longitudinal waves, γ = heterogeneous flow, and ϵ = homogeneous flow. The beginning of the α regime appears to coincide with the initiation of particle movement and is shown by the solid curve extending from the lower left to the upper right of Figure 3. This curve is independent of tube diameter, and the effect of particle density is completely accounted for by the density term in the hindered-settling velocity. The end of the α regime (or the beginning of the β regime) is also independent of tube diameter but now requires an additional factor to account for the particle density for $D_p u_o^*/\nu > 5$. The value of this factor is tentatively of the form given by Equation (4). For values of the parameter ($D_p u_o^*/\nu$) < 3 the end of the β regime is independent of pipe diameter, and the particle density is accounted for by the terminal-settling velocity [Equation (2)]. For $D_p u_o^*/\nu > 5$ and $D u_o^*/\nu > 260$ the end of the β regime is a function of tube diameter, and an additional density term is required [Equation (3)]. The curves shown in Figure 3 are for tube diameters of 1, 4, and 12 in. and for a value of the parameter $(\rho_p - \rho)/\rho = 1.65$. Curves for different density values may be prepared by scaling Figure 3 in accordance with Equation (4).

The end of the γ regime (heterogeneous flow) and the beginning of the ϵ regime (homogeneous flow) is difficult to arrive at because of the paucity of experimental and theoretical results and the difficulty of defining these flow conditions. For very fine particles in the micron size range considerable data (*11, 14, 17*) indicate that substantially homogeneous flow is achieved as soon as the minimum transport velocity is exceeded, for example the data on the lower left of Figure 1. For larger sized particles Newitt et al. (*24*) have proposed an expression for the beginning of homogeneous flow which may be converted to the dimensionless form of the present paper by Equation (6):

$$\frac{U_t}{u_H^*} = 0.0148 \left(\frac{2}{f}\right)^{5/8} \left(\frac{D_p u_H^*}{\nu}\right)^{2/3} \left(\frac{\nu}{D u_H^*}\right)^{0.42} \left(\frac{\rho_s - \rho}{\rho}\right)^{0.42} \tag{8}$$

The only concentration distribution data for solids in liquids that permit a check of this expression are those of Barnard and Binnie (*6*) for transport of particles near the neutral density condition. For one particular set of data the ratio of the probability density values for particle distribution within one particle radius of the top and bottom of the pipe was 0.35 (that is not completely uniform but an appreciable fraction of the spheres were in the upper portion of the pipe). Under these conditions Equation (8) predicts that a homogeneous suspension would be achieved at a friction velocity 1.96 times the value existing for the above test. Although this is far from being a desirable check of Equation (8), in the absence of more data it does indicate that Equation (8) predicts values in the right direction. Curves calculated from Equation (8) for pipe diameters of 1 and 4 in. and a value of the parameter $(\rho_p - \rho)/\rho = 1.65$ are shown on Figure 3 to indicate the approximate region where homogeneous flow may be expected.

The increase in velocity required to achieve homogeneous transport, once the minimum transport condition is known, can be obtained from the ratio of Equations (3) and (8):

$$\frac{u_H^*}{u_{om}^*} = 97 \frac{f}{2} \left(\frac{D_p u_{om}^*}{\nu}\right)^{0.12} \left(\frac{D_p}{D}\right)^{0.15} \left(\frac{\rho}{\rho_p - \rho}\right)^{0.15} \tag{9}$$

For the rather wide range of values, $5 < (D_p u_{om}^*/\nu) < 10^3$, $10^{-3} < (D_p/D) < 0.15$, and $0.09 < (\rho_s - \rho)/\rho < 9$, Equation (9) gives

$$1.5 < u_H/u_{om}^* < 11.8 \tag{10}$$

or less than a tenfold range.

Another velocity of interest in suspension transport is the rather arbitrary standard velocity V_s. A correlation proposed by Spells (*27*) for the standard velocity may be converted to the form of the present paper with Equation (6):

$$\frac{U_t}{u_s^*} = 13.5 \left(\frac{D_p u_s^*}{\nu}\right)^{0.43} \left(\frac{\nu}{D u_s^*}\right)^{0.55} \tag{11}$$

Taking the ratio of Equations (3) and (8) and evaluating the limits for the ranges given above one obtains

$$0.75 < u_s^*/u_{om}^* < 19 \tag{12}$$

a somewhat wider range than that obtained for the homogeneous transport ratio Equation (10).

MECHANISM OF PARTICLE TRANSPORT

The flow regime diagram presented in this paper describes four readily identifiable modes for suspension transport based on empirical observations. As yet there is no general theoretical treatment which adequately describes the various flow conditions. However analysis of specific flow regimes gives some insight into possible mechanisms of suspension transport.

Transverse Wave Regime

Liu (*21*) recognized that the beginning of bed load movement and ripple formation in alluvial channels occurred virtually simultaneously. He also showed that by equating the erosive force of the flow and the resistance force of the particles the beginning of transverse wave formation is given by an expression of the form

$$U_t/u^* = \psi (D_p u^*/\nu) \tag{13}$$

which is just the unique relation shown in Figures 2 and 3. A detailed analysis of the mechanics of transverse wave formation based on the present studies will be given in a subsequent paper.

Minimum Transport Condition

For particles with a diameter $D_p/\delta < 1$ the observed

TABLE 2. RANGE OF DATA ON WHICH FLOW REGIME DIAGRAM IS BASED

Regime	Particle diameter, μ	Particle density, g./cc.	Fluid	Pipe diameter, in
α: Transverse waves	50 to 4240	1.09 to 2.65	Water	¼ to 4
β: Longitudinal waves	59 to 950	1.09 to 2.65	Water	¼ to 4
γ: Heterogenous flow				
$(D_p u_*/\nu) < 5$	0.74 to 78	1.35 to 10	Air and water	½ to 4
$(D_p u_*/\nu) > 5$	97 to 38,100	1.08 to 11.3	Air and water	½ to 32
ϵ: Homogeneous flow	100 to 6,000	1.18 to 4.60	Water	¾ to 1

minimum transport velocity was shown to be consistent with the values predicted from a force balance in which the Bernoulli force due to the large velocity gradient near the wall was equated to the gravitation force on the particle (*11*). No analysis accompanied the empirical correlation for the minimum transport velocity of larger sized particles (*11*). One possible mechanism is that the minimum transport velocity occurs when the turbulent fluctuations of the fluid are sufficiently large to impart an upward acceleration to the particles that just overcomes the gravitational force on the particles. An estimate of the force on the particles due to the turbulence may be obtained from the theory of local isotropy (*28*). Strictly speaking this theory is valid only for flows in which there is no mean velocity gradient. Corrsin (*29*) has suggested that the theory may be applied to shear flows when the local transfer time is shorter than the characteristic time of the gross shear strain, or that $(\epsilon/\nu)^{1/2} >> \partial V/\partial y$. This criterion is often fulfilled for the central portion of flow in a channel provided the Reynolds number is sufficiently large. On this assumption an expression developed by Yaglom (*30*) may be used to calculate the value of the local accelerations due to the turbulence. For $\mathcal{L} >> r >> \eta$ the local acceleration of a fluid element

$$W_r = (\epsilon^2/r)^{1/3} \tag{14}$$

may be derived from dimensional considerations (*30*). The integral scale $\mathcal{L}$ is roughly proportional to the radius of the pipe (*31*) with the constant of proportionality in the range 1/20 to 1/2, while the Kolmogoroff characteristic length scale is $\eta = (\nu^3/\epsilon)^{1/4}$. On the assumption that in order to be effective the region for which the local acceleration [Equation (14)] applies is of the same order as the particle size, then a simple force balance gives for the minimum transport condition

$$\epsilon^{2/3} = g_L D_p^{1/3} (\rho_p - \rho)/\rho \tag{15}$$

For pipe flows ϵ may be estimated from

$$\epsilon = 2f\frac{V^3}{D} \tag{16}$$

which assumes that the core of the flow is nearly homogeneous and dissipates most of the energy (*32*). Combining Equations (6), (15), and (16) one gets an approximate expression for the minimum transport condition in the same form as used in the present paper:

$$\frac{U_t}{u^*_{om}} = 1.15\left(\frac{D_p u^*_{om}}{\nu}\right)^{0.09}\left(\frac{\nu}{D u^*_{om}}\right)^{0.47} \tag{17}$$

This relation is in good agreement with the experimental data for liquid suspensions if the numerical constant is increased to 1.82.

ENGINEERING APPLICATIONS

The correlations upon which flow regime diagrams, such as Figure 3, are based were derived from a large amount of data taken with an extremely wide range of system characteristics. The extent of the range of data for the different flow regimes is given in Table 2.

The one factor not included in Table 2 is that the present data for the onset of island formation in round pipes with the larger particle sizes is corroborated by the data for onset of ripple formation in streams and alluvial channels (*20, 21*).

The data for the minimum transport correlation include results for both air and water as well as a wide range of particle and pipe diameters. This velocity has been recommended as the optimum for design of systems for suspension transport by many investigators (*25, 35, 38*). In fact substitution of data from the literature (*39, 40*) for mean particle size, pipe diameter, and concentration into the minimum transport correlation of Part VI of this series (*11*) gave a velocity which was within 10% the value actually used in the successful operation of the 108-mi. long, 10-in. diameter coal suspension pipeline. Consequently although additional work may change some details of the flow regime diagram, particularly the limit on homogeneous flow, it can be used with confidence for most applications.

Once a flow regime diagram for a particular value of $(\rho_p - \rho)/\rho$ is available, many problems of interest can be solved rather rapidly. As an example consider the determination of the velocities corresponding to the different flow regimes for a particle of density 2.65 and diameter of 375 μ with water at 70°F. as the fluid. The first step is to determine the particle Reynolds number $D_p U_t/\nu$. The terminal-settling velocity can be calculated from either Equations (5), (6), or (7), or it can be determined from available charts (*26*); the result is $U_t = 0.172$ ft./sec., corresponding to a Reynolds number of 20. When one follows the line for $N_{Re} = 20$ from left to right on Figure 3, the values of $D_p u_o^*/\nu$ corresponding to the beginning of the different regimes can be read from the intersection with the appropriate lines. The value of u_o^* can be determined immediately since both D_p and ν are known. The values of the mean stream velocity may be calculated from

$$V = u_o^* \sqrt{2/f} \tag{18}$$

Velocities for the onset of the different flow regimes calculated by the above procedure are given in Table 3.

Care must be used in applying the flow regime diagram under certain conditions. At the lowest flow rates, if the layer of solids on the bottom of the pipe is greater than 0.1- to 0.25-pipe diameters deep, the solids may accumulate into a large mound which moves down the pipe at a mean stream velocity less than that given by the flow regime diagram owing to the constriction in the flow caused by the large mound. Also there is a concentration correction that must be applied at the minimum transport condition (*11*). However Newitt's data (*24*) seem to indicate that the condition for homogeneous flow is independent of concentration. The distinction between heterogeneous and homogeneous flow is arbitrary and rather poorly understood at present. Additional experimental and

TABLE 3. VELOCITIES FOR ONSET OF DIFFERENT FLOW REGIMES FOR 375-μ PARTICLES OF DENSITY 2.65 G./CC. IN 70°F. WATER

Flow regime	Friction velocity, ft./sec. Tube diam., 1 in.	Friction velocity, ft./sec. Tube diam., 4 in.	Mean stream velocity, ft./sec. Tube diam., 1 in.	Mean stream velocity, ft./sec. Tube diam., 4 in.
Transverse waves	0.0474	0.0474	0.71	0.87
Longitudinal waves	0.101	0.101	1.70	2.05
Heterogeneous flow	0.129	0.239	2.25	5.35
Homogeneous flow	0.482	0.767	9.9	19.4

theoretical work in this area are to be desired. The designation of the region $y^+ < 5$ [Equation (1)] as the laminar sublayer is somewhat arbitrary, since in reality some turbulent fluctuations appear to extend virtually to the wall (28). In fact the present data appear to show a break at $D_p u_o^*/\nu = 3$ rather than at a value of 5 as might be expected. Consequently the location of the vertical line for $D_p/\delta = 1$ on Fig. 3 may actually be at $D_p u_o^*/\nu = 3$ rather than as indicated. Additional work is required to clarify the location and the nature of the flow phenomena in this region.

ACKNOWLEDGMENT

Work was performed for the Office of Saline Water, United States Department of Interior, at the Oak Ridge National Laboratory operated by the Union Carbide Corporation for the United States Atomic Energy Commission.

NOTATION

C = concentration, arbitrary units
D = pipe diameter, ft.
D_p = particle diameter, ft.
f = Fanning friction factor, $(D\Delta p/4L)/(\rho V^2/2g_c)$ dimensionless
g_c = conversion factor, (lb.$_m$/lb.$_f$) (ft./sec.^{2})
g_L = gravitational acceleration, ft./sec.^{2}
Δh = head loss in feet of fluid flowing, ft.
L = length, ft.
$\mathcal{L}$ = integral scale, ft.
Δp = pressure drop, lb.$_f$/sq. ft.
r = radial position, ft.
R = tube radius, ft.
U_t = terminal-settling velocity, ft./sec.
u^* = fraction velocity, $\sqrt{g_c D \Delta p/4\rho L}$, ft./sec.
V = fluid velocity, ft./sec.
y = distance, ft.
y^+ = distance, $y u^*/\nu$, dimensionless

Greek Letters

δ = laminar sublayer thickness, $y^+ = 5$, dimensionless
ϵ = local rate of energy dissipation, sq. ft./sec.^{3}
η = Kolmogoroff length, ft.
μ = viscosity, lb.$_m$/ft. sec.
ν = kinematic viscosity, sq. ft./sec.
ρ = density, lb.$_m$/cu. ft.
ψ = function of

Subscripts

a = average
B = beginning of particle movement
H = homogeneous flow
m = minimum transport
o = infinite dilution
p = particle
s = standard velocity

LITERATURE CITED

1. Tchen, Chan-Mou, "Mean Value and Correlation Problems Connected with the Motion of Small Particles Suspended in a Turbulent Fluid," Martinus Nijhoff, The Hague (1947).
2. Soo, S. L., *Chem. Eng. Sci.*, **5**, 57 (1956).
3. Soo, S. L., *Ind. Eng. Chem. Fundamentals*, **1**, 33 (1962).
4. Lumley, J. L., Ph.D. thesis, Johns Hopkins Univ., Baltimore, Maryland (1957).
5. Peskin, R. L., "1960 Heat Transfer and Fluid Mechanics Institute," Stanford University Press, Stanford, California (1960).
6. Barnard, B. J. S., and A. M. Binnie, *J. Fluid Mech.*, **15**, 35 (1963).
7. Houghton, G., *Brit. J. Appl. Phys.*, **13**, 17 (1962).
8. Zenz, F. A., and D. F. Othmer, "Fluidization and Fluid Particle Systems," Reinhold, New York (1960).
9. Anderson, A. G., "Handbook of Fluid Dynamics," Chap. 18, Streeter, V. L., ed., McGraw-Hill, New York (1961).
10. Vanoni, V. A., N. H. Brooks, and J. F. Kennedy, *W. M. Keck Laboratory of Hydraulics and Water Resources Report KH-Rl*, California Institute of Technology, Pasadena, California (January, 1961).
11. Thomas, D. G., *A.I.Ch.E. Journal*, **7**, 423 (1961); **8**, 373 (1962).
12. Soo, S. L., and J. A. Regalbuto, *Can. J. Chem. Eng.*, **38**, 160 (1960).
13. Blatch, N. S., *Trans. Am. Soc. Civil Engrs.*, **57**, 400 (1906).
14. Durand, R., "Proceedings of Minnesota Hydraulic Convention," Part 1, pp. 89-103, Univ. Minnesota (1953).
15. Zenz, F. A., *Ind. Eng. Chem.*, **41**, 2801 (1949).
16. Bagnold, R. A., "Physics of Blown Sand and Desert Dunes," Methuen, London, England (1941).
17. Cairns, R. C., K. R. Lawther, and K. S. Turner, *Brit. Chem. Eng.*, **5**, 849 (1960).
18. Gibert, R., *Annales des Ponts and Chaussees*, p. 307 (May-June, 1960).
19. Kraus, K. A., Personal communication (April 4, 1963); *J. Am. Chem. Soc.*, **80**, 4154 (1958).
20. Shields, A., "Mitt preuss. Versuchanstalt Wasserbau u. Schiffbau," Berlin, Germany (1936).
21. Liu, H. K., *Trans. Am. Soc. Civil Engrs.*, **121**, 877 (1956).
22. Zenz, F. A., *Ind. Eng. Chem. Fundamentals*, **3**, 65 (1964).
23. von Karman, Theodore, *J. Aeronaut. Sci.*, **1**, 1 (1934).
24. Newitt, D. M., J. F. Richardson, M. Abbott, and R. B. Turtle, *Trans. Inst. Chem. Engrs.*, **33**, 93 (1955).
25. Worster, R. C., and D. F. Denny, *Proc. Inst. Mech. Engrs.*, **169**, 563 (1955).
26. Lapple, C. E., "Chemical Engineer's Handbook," 3 ed., 1021, Perry, J. M., ed., McGraw-Hill, New York (1950).
27. Spells, K. E., *Trans. Inst. Chem. Engrs.*, **33**, 80 (1955).
28. Hinze, J. O., "Turbulence," McGraw-Hill, New York (1960).
29. Corrsin, Stanley, *Natl. Aeronaut. Space Administration Rept. RM-58-B-11* (May 28, 1958).
30. Obukhoff, A. M., and A. M. Yaglom, *Prik. Matematika i Mekhanika*, **15**, 3 (1951).
31. Corrsin, Stanley, *J. Geophys. Res.*, **64**, 2134 (1959).
32. Taylor, G. I., "Advances in Geophysics" p. 110, Frenkiel, F. N., and P. A. Sheppard, ed., Academic Press, New York (1959).
33. Thomas, D. G., *Science*, to be published.
34. Newitt, D. M., J. F. Richardson, and C. A. Shook, "Proceedings of Symposium on the Interaction between Fluids and Particles," p. 87, Rottenberg, P. A., ed., The Institution of Chemical Engineers, London, England (1963).
35. Sinclair, C. G., *ibid.*, p. 79.
36. Soo, S. L., *ibid.*, p. 72.
37. Heywood, H., *ibid.*, p. 1.
38. Condolios, Elie, and E. E. Chapus, *Chem. Eng.*, **70**, No. 13, p. 131 (July 8, 1963).
39. Dauber, C. A., *Combustion*, **28**, No. 10, p. 39 (April, 1957).
40. Anon, *Mining Eng.*, **14**, No. 1, p. 48 (January, 1962).

Manuscript received June 27, 1963; revision received August 19, 1963; paper accepted August 23, 1963.